Available online at www.sciencedirect.com
SCIENCE DIRECT®
International Journal of Thermal Sciences 43 (2004) 145–155
International Journal of Thermal Sciences
www.elsevier.com/locate/ijts

A numerical solution of the linear multidimensional unsteady inverse heat conduction problem with the boundary element method and the singular value decomposition

G.L. Lagier, H. Lemonnier *, N. Coutris

DTP/SMTH/LDTA, Commissariat à l'Energie Atomique Grenoble, 38054 Grenoble cedex 9, France

Received 30 October 2001; accepted 16 June 2003

Abstract

In this paper, we present a new method for solving the general linear multidimensional unsteady inverse heat conduction problem. The direct numerical method is based on the Boundary Element Method formulation. Taking into account future time steps, the ill-conditioned linear system is solved using a procedure based on the Singular Value Decomposition technique which handles both spatial and temporal instabilities. The regularization method is essentially a spectral truncation method with a single hyperparameter. The optimal value of this hyperparameter can be chosen *a priori* from the knowledge of the data uncertainty.

In the second part of this paper, an experiment is described which illustrates an application of the method on a two-dimensional problem. The physical problem consists in identifying the heat flux on a plate exposed to a moving front of hot fluid from temperature measurements collected on the opposite side of the plate. Numerical results obtained are discussed in comparison to direct heat flux measurements. The purpose of this experiment was to cross-check two types of heat flux sensors in real unsteady two-dimensional situations. It is also shown that the method can be applied to real 3D problems.

Keywords: Inverse problem; Time and space regularization; Singular value decomposition; Experiments

1. Introduction

The Inverse Heat Conduction Problem (IHCP), like the vast majority of inverse problems, is known to be ill-posed: besides the possible non-uniqueness of the solution of discretized problem, the results are very sensitive to input data noise. In order to get significant results, regularization procedures must be used when solving the linear system associated to the problem. It is known that many steady inverse problems are already ill-posed [7,8]. Moreover, for unsteady inverse problems, due to parabolic nature of the heat diffusion equation, additional time related phenomena such as damping and lagging effects increase the sensitivity of solution to measurement errors.

To cope with the lagging effect of the diffusion operator, many methods such as the function specification method have been used [2]. These methods acknowledge that temperatures at a given time and location depend only very slightly on neighboring temperatures values at the same time; whereas temperature values at earlier times may depend more significantly on these former temperatures. Therefore, it is important not to solve only in sequential manner at time t for the unknown values of the temperature, but to solve for all the temperature values within a given time range in the past to improve the conditioning of the problem. It is often referred to these methods as the "future time steps" method, since a temperature value at time t is significantly dependent on temperatures values at time $t - \tau$. When reversing the point of view and considering past temperature values, they seem to depend on future temperature values.

As a consequence, many authors have developed multidimensional algorithms based on a two-fold regularization procedure. For steady problems, the Tikhonov technique [12], and iterative gradient methods [1] are widely used. For unsteady problems, the function specification

* Corresponding author.
E-mail address: herve.lemonnier@cea.fr (H. Lemonnier).

1290-0729/$ – see front matter
doi:10.1016/j.ijthermalsci.2003.06.002

Nomenclature

a	spatial decay of heat flux distribution see Eq. (25) ..... $m{\cdot}s^{-1}$
$\mathbf{A}$	boundary element discretised operator of the sequential direct problem
$\mathbf{b}$	vector of the known part of Eq. (9)
c	boundary function defined in Eq. (3)
$\mathbf{C}$	matrix, the coefficients of which are defined in Eq. (7)
d	space dimension, $d \in \{1, 2, 3\}$
e	wall thickness..... m
F	number or time steps
Fo	Fourier number, non-dimensional, $Fo = t/t_0$
G_t	Green's function defined in Eq. (5)
$\mathbf{G}$	matrix, the coefficients of which are defined in Eq. (6)
H	Heaviside function
$\mathbf{H}$	matrix the coefficients of which are defined in Eq. (6)
k	thermal conductivity ..... $W{\cdot}m^{-1}{\cdot}K^{-1}$
K	condition number of the designated matrix, see Eq. (16)
q	heat flux..... $W{\cdot}m^{-2}$
$\mathbf{q}$	vector of the boundary heat flux values
t	time ..... s
T	temperature, non-dimensional unless otherwise stated ..... K
M	observer point
M'	source point
N	number of boundary elements
N_{pf}	number of future time steps
N_{pi}	number of internal collocation points
$\mathbf{n}$	outwardly oriented normal vector on the boundary, length = 1
P	number of unknown boundary values
t_0	diffusion time scale, defined in Table 1 ..... s
$\mathbf{T}$	vector of the boundary temperature values
w	singular value
$\mathbf{U}$	orthogonal matrix, base of the source space
v	rise velocity in the Cinthia experiment.. $m{\cdot}s^{-1}$
v_0	diffusion velocity scale, defined in Table 1 ..... $m{\cdot}s^{-1}$
$\mathbf{V}$	orthogonal matrix, base of the image space
$\mathbf{W}$	diagonal singular value matrix
x	observer point
x'	source point
y	vector of the unknown boundary values (temperature or heat flux)

Greek letters

α	heat diffusivity ..... $m^2{\cdot}s^{-1}$
Δ	uncertainty of the designated variable
ε	threshold on the singular values, truncation level
μ	hyperparameter of the Tikhonov regularization
τ	time interval $(t_F - t)$ ..... s

Subscripts, and superscripts

$*$	non-dimensional, time scale is t_0
t	transpose of a matrix
F	final or resolution time
f	relative to time step

Operators

Δ	Laplacian operator
$\mathcal{L}$	linear heat diffusion operator, see Eq. (1)

method developed by Beck et al. [2] is often used in tandem with one of the two previously mentioned methods. In addition it must be mentioned that Pasquetti and Le Niliot [10] have also implemented a temporal Tikhonov regularization method.

The novelty of our method is to use a single regularization procedure for dealing with both temporal and spatial instabilities. It is based on the Singular Values Decomposition technique. In the first part of this paper the boundary element formulation of the problem is shortly introduced. Next, the regularization procedure is developed and the choice of the regularization parameters are discussed. Finally an illustration of our method is presented on selected analytical test cases and real experiments. The results are compared to existing regularization methods such as the Tikhonov method of order 0 [12] and heat flux direct measurements. Finally, the proposed method is also shown to be directly applicable to real 3D problems.

2. Description of the method

2.1. Direct problem: Boundary element method (BEM)

The advantages of the boundary element method are now well known in the field of inverse problems in heat conduction [10]. Only the boundary of the domain has to be discretized and internal points are explicitly excluded from the solution procedure. An interesting side effect is the considerable reduction in size of the linear system to be eventually solved. One can also note that the heat flux is the main variable of the problem, unlike other numerical methods where the temperature is the only independent variable. The limitation to a linear diffusion problem (uniform thermal diffusion throughout the domain) is the price to pay for this, although significant departure from this limitation is still possible such as the multiple reciprocity method de-

scribed by Novak and Newes [9]. Let us now consider the general multi-dimensional heat diffusion equation,

$$\mathcal{L}T = \Delta T - \frac{1}{\alpha}\frac{\partial T}{\partial t} = 0 \tag{1}$$

$$T = T_0, \quad \text{throughout the domain at time } t = 0 \tag{2}$$

where $\mathcal{L}$ is the linear heat diffusion operator, T is the temperature, α is the thermal diffusivity, Δ is the Laplacian operator and T_0 is the initial temperature distribution at time $t = 0$ and where the explicit expression of the Laplacian operator depends on the specific problem of interest. In particular, when the initial temperature field, T_0, is harmonic, the knowledge of a fundamental solution of Eq. (1) with a localized and impulsive heat source, G_t (a free space Green's function of the adjoint operator) yields an integral formulation equivalent to Eq. (1). Integrating the product of $\mathcal{L}T$ and G_t on the domain and in time from the initial time, $t = 0$, and any given final time, t_F, and using the second Green's identity and further integrating by parts in time the result, one obtains,

$$c(x)T(x,t_F) = \int_0^{t_F}\int_{\partial\Omega} \alpha G_t \frac{\partial T}{\partial n}\mathrm{d}(\partial\Omega)\,\mathrm{d}t - \int_0^{t_F}\int_{\partial\Omega} \alpha T \frac{\partial G_t}{\partial n}\mathrm{d}(\partial\Omega)\,\mathrm{d}t \tag{3}$$

$$c(M') = \begin{cases} 1 & M' \in \Omega \\ 1/2 & M' \in \partial\Omega \end{cases} \tag{4}$$

where G_t is a fundamental solution of the adjoint problem, with a ponctual heat source located at x' and activated at time t_F which can be written as,

$$G_t = G_t(x, x' \mid t, t_F) = \frac{1}{(4\pi\alpha\tau)^{d/2}}\exp\left(-\frac{r^2}{4\alpha\tau}\right)H(\tau) \tag{5}$$

where r is the distance between the source point and the field point, $\tau = t_F - t$, d is the space dimension (1, 2 or 3) and $H(\tau)$ denotes the Heaviside function. When sources are present or the initial temperature field is not harmonic, a boundary only formulation is not generally possible.

To solve the governing equation (3), a time and space discretization scheme is needed and the discretised equation is solved by a collocation method. The boundary is divided into N elements (which are points in 1-D, segments in 2-D and polygonal elements in 3-D) and F time steps are considered. The unknowns are assumed to be uniform on every element, $\partial\Omega_j$ $(j = 1,\ldots,N)$, and constant on each time step $[t_{f-1}, t_f]$ $(f = 1,\ldots,F)$, and equal to the value of the unknown at the center of gravity, x_j, of the element and at the final time, t_f, of the considered time step. Finally, we obtain the following set of linear equations,

$$c_i T_{i,F} = \sum_{f=1}^{F}\sum_{j=1}^{N} H_{ij,Ff}T_{j,f} = \sum_{f=1}^{F}\sum_{j=1}^{N} G_{ij,Ff}q_{j,f} \tag{6}$$

with the following notations,

$$\begin{aligned} &c_i = c(x_i), \qquad T(x_j,t_f) = T_{j,f} \\ &\frac{\partial T}{\partial n}(x_j,t_f) = q_{j,f} \end{aligned} \tag{7}$$

$H_{ij,Ff}$ and $G_{ij,Ff}$ are some coefficients resulting of a time and space integration. Lagier [5] developed computationally efficient and accurate algorithms to compute them in most of the useful element configurations including spherical and cylindrical symmetric systems. Writing Eq. (6) for every selected boundary point and every internal point of interest, and introducing matrices $\mathbf{H}$ and $\mathbf{G}$, one obtains the so-called sequential BEM formulation:

$$\mathbf{C}\mathbf{T}_F + \sum_{f=1}^{F}\mathbf{H}_{Ff}\mathbf{T}_f = \sum_{f=1}^{F}\mathbf{G}_{Ff}\mathbf{q}_f \tag{8}$$

When solving the problem at time t_F, all the temperatures and heat fluxes are known until time t_{F-1}. Finally, taking the boundary conditions into account, one can separate the known values of the heat flux or the temperature and the unknown variables among the components of $\mathbf{T}_F$ and $\mathbf{q}_F$. By grouping the unknown values in a single vector, $\mathbf{y}_F$, the following linear system of $N + N_{pi}$ equations in P unknowns is obtained,

$$\mathbf{A}_{FF}\mathbf{y}_F = \mathbf{b}_F \tag{9}$$

As mentioned above, when we deal with inverse problems, "future" temperatures may be used to take into account the lagging effect of the diffusion operator. Then, to determine $\mathbf{y}_F$, Eq. (9) is written not only at time t_F but also at N_{pf} future time steps. So, the final linear system to be solved consists of $(N + N_{pi})(N_{pf} + 1)$ equations in $P(N_{pf} + 1)$ unknowns, which in matrix form becomes,

$$\begin{pmatrix} \mathbf{A}_{FF} & 0 & \cdots & 0 \\ \mathbf{A}_{(F+1)F} & \mathbf{A}_{(F+1)(F+1)} & \cdots & 0 \\ \vdots & \vdots & \ddots & 0 \\ \mathbf{A}_{(F+Npf)F} & \mathbf{A}_{(F+Npf)(F+1)} & \cdots & \mathbf{A}_{(F+Npf)(F+Npf)} \end{pmatrix} \times \begin{pmatrix} \mathbf{y}_F \\ \mathbf{y}_{F+1} \\ \vdots \\ \mathbf{y}_{F+Npf} \end{pmatrix} = \begin{pmatrix} \mathbf{b}_F \\ \mathbf{b}_{F+1} \\ \vdots \\ \mathbf{b}_{F+Npf} \end{pmatrix} \tag{10}$$

If the time step is chosen to be a constant then a simplified system is obtained,

$$\begin{pmatrix} \mathbf{A}_{00} & 0 & \cdots & 0 \\ \mathbf{A}_{10} & \mathbf{A}_{00} & \cdots & 0 \\ \vdots & \vdots & \ddots & 0 \\ \mathbf{A}_{Npf0} & \mathbf{A}_{(Npf-1)0} & \cdots & \mathbf{A}_{00} \end{pmatrix} \begin{pmatrix} \mathbf{y}_F \\ \mathbf{y}_{F+1} \\ \vdots \\ \mathbf{y}_{F+Npf} \end{pmatrix} = \begin{pmatrix} \mathbf{b}_F \\ \mathbf{b}_{F+1} \\ \vdots \\ \mathbf{b}_{F+Npf} \end{pmatrix} \tag{11}$$

It should be noted that in this particular, but very common case, where the boundary conditions are linear with the temperature, the linear system has to be solved only once whatever the number of time steps. This results directly from the dependency of G_t in τ only. However, the block triangular form of Eq. (11) suggests that the discretised problem remains parabolic in nature as the solution does not depend on the future. Without regularization, Eq. (11) is strictly equivalent to the ordinary sequential formulation of Eq. (9) since the evolution of the solution is not specified. The regularization procedure will now be applied directly to Eq. (10) or Eq. (11). The ill-conditioning of matrix **A** is a consequence of the ill-posedness of this inverse problem. Finally, our method being sequential, the linear system given by Eq. (11) is solved step by step in a sequential manner. However, only the values of $\mathbf{y}_F$ are stored at time t_F.

Convergence in time and space of the method has been checked by a systematic comparison with analytical solutions. It has been shown by Lagier [5] that the RMS error on boundary temperature follows the following equation,

$$\text{RMS Error} = A\Delta t + B\Delta x^2 \tag{12}$$

where A and B are positive constants depending on the specific problem studied, Δt is the time step and Δx is the element length, which has been selected to be uniform for the purpose of the convergence study only. In addition with Eq. (12) the following recommendation has been issued by Lagier [5],

$$\frac{\alpha\Delta t}{\Delta x^2} = \mathrm{O}(1) \tag{13}$$

This result physically means that the time required for heat to diffuse on a length Δx should be of the order of the time step Δt. Using this latter criterion, it results that the two contributions in the error equation (12) have the same magnitude.

2.2. Regularization procedure: The singular value decomposition technique (SVD)

The singular values decomposition technique [3,11] is a general purpose method for solving discrete ill-conditioned problem. It has already been successfully used for solving steady inverse heat conduction problems [4,7]. The goal of this regularization method is to eliminate the components of the solution prone to corruption by the input data errors. Indeed, by definition of the SVD of a matrix **A**, we have,

$$\mathbf{A} = \mathbf{U}\cdot\mathbf{W}\cdot\mathbf{V}^t \tag{14}$$

where **W** denotes the diagonal singular value matrix, every diagonal element w_i being the i th singular value, greater than or equal to 0, and **U** and **V** are both orthogonal matrices, i.e., $\mathbf{U}^t\cdot\mathbf{U} = \mathbf{I}$ and $\mathbf{V}^t\cdot\mathbf{V} = \mathbf{I}$. The geometrical interpretation of the SVD is straightforward when two particular bases are considered: (i) the base of the space where **b** lies which is generated by the columns of **U** and (ii) the base of the space where **y** lies which is generated by the columns of **V**. If **b** is the image of **y** through **A** then the component of **b** along $\mathbf{U}_i$ is the component of **y** along $\mathbf{V}_i$ multiplied by the ith singular value, w_i. Solving **A** in these bases is therefore straightforward.

For a non-singular squared matrix, the solution of a linear set of equation such as Eq. (9) by using the SVD technique is given by:

$$\begin{aligned}\mathbf{V}^t\mathbf{y} &= \begin{pmatrix} w_1^{-1} & 0 & 0 \\ 0 & \dots & 0 \\ 0 & 0 & w_n^{-1} \end{pmatrix}\mathbf{U}^t\mathbf{b} \\ \Longleftrightarrow \mathbf{y} &= \mathbf{V}\begin{pmatrix} w_1^{-1} & 0 & 0 \\ 0 & \dots & 0 \\ 0 & 0 & w_n^{-1} \end{pmatrix}\mathbf{U}^t\mathbf{b}\end{aligned} \tag{15}$$

where n is the number of non-zero singular values of **A**. In addition the SVD technique provides an explicit bounding of the uncertainty on the results when the uncertainty of the input data is known. These are related by the following inequality,

$$\frac{\|\Delta\mathbf{y}\|}{\|\mathbf{y}\|} \leqslant \frac{w_{\max}}{w_{\min}}\frac{\|\Delta\mathbf{b}\|}{\|\mathbf{b}\|} = K(\mathbf{A})\frac{\|\Delta\mathbf{b}\|}{\|\mathbf{b}\|} \tag{16}$$

where $K(\mathbf{A})$ is the condition number of the matrix **A**.

In inverse problems, the matrix **A** is ill-conditioned, i.e., it is singular or close to being singular; some singular values are very small or equal to zero. As a result, input data noise is greatly amplified in the corresponding singular or close to singular directions ($\mathbf{V}_i$) of the solution. The advantage of the SVD regularization is to identify these directions which are prone to corruption. Therefore, it is very simple to project the solution on the subspace spanned by the remaining directions by formally replacing w_i^{-1} by 0 in (15). Therefore, the regularized solution of (11) is reconstructed from its projections by,

$$\begin{aligned}&\left(\mathbf{V}^t\cdot\mathbf{y}\right)_i = w_i^{-1}\cdot\left(\mathbf{U}^t\cdot\mathbf{b}\right)_i \quad \text{if } w_i \geqslant \varepsilon \\ &\left(\mathbf{V}^t\cdot\mathbf{y}\right)_i = 0 \qquad\qquad\qquad\quad \text{if } w_i < \varepsilon\end{aligned} \tag{17}$$

where ε is the so-called singularity threshold. This hyperparameter must be chosen to provide the best compromise between the loss of information due to the partial splitting of matrix **A** and the input data noise amplification resulting from the small values of the last singular value considered. This is basically the same type of reasoning on which relies the "L-curve" methodology [3]. It should be noted that a sensitivity analysis on ε can be easily realized since only one SVD of matrix **A** is needed: changing the value of the hyperparameter does not require to restart the calculation from scratch.

Consider now the non-dimensional problem, Lagier [5] proposed simple scaling methods based on the relevant scales of the problem. They can be found readily from the length of the domain and the initial and boundary conditions of the problem. For example, if the thermal shock on a wall is considered, the thickness of the wall is the relevant length scale of the problem and the temperature scale depends on

the initial and boundary conditions. Let us consider on one hand, a thermal shock with a imposed temperature, T_1, on one side of the wall initially at temperature T_0, then the temperature scale is $T_1 - T_0$. On the other hand if the heat flux, q_0, is imposed, the temperature scale is eq_0/k where k it the thermal conductivity of the wall material. By using these scales, non-dimensional temperatures and fluxes are of order unity.

If the **A** matrix is considered, the relation between the uncertainty of the solution and that of the data is given by Eq. (16). Now if the p largest singular values are only considered, i.e., the SVD decomposition of **A** is truncated, then Lagier [5] have proved the following inequality,

$$\frac{\|\Delta \mathbf{y}\|}{\|\mathbf{y}\|} \leqslant \frac{w_{\max}}{w_p} \frac{\|\Delta \mathbf{b}\|}{\|\mathbf{b}\|} + 1 \tag{18}$$

This equation means that the error on the stabilized solution using SVD regularization can be seen as the weighted sum of the uncertainty due to input data noise and the uncertainty resulting from the truncation of the operator by discarding from the solution the subspace spanned by $\{\mathbf{V}_i,\ i = p+1, \ldots, n\}$. The parameter ε thresholding the spectrum of the singular values is related to p by,

$$w_p > \varepsilon > w_{p+1} \tag{19}$$

The parameter ε is next chosen so that both noise uncertainty and truncation uncertainty have the same weight. This provides,

$$\varepsilon = w_{\max} \frac{\|\Delta \mathbf{b}\|}{\|\mathbf{b}\|} \tag{20}$$

Next, it can be shown that **b** being a linear combination of temperatures and heat fluxes, the uncertainty on **b** is related to that of the non dimensional temperature by,

$$\frac{\|\Delta \mathbf{b}\|}{\|\mathbf{b}\|} = \frac{\|\Delta \mathbf{T}^*\|}{\|\mathbf{T}^*\|} \tag{21}$$

Finally, the uncertainty on the temperature can be characterized by the standard mean deviation of the temperature measurements, σ_T. This value is an index of quality of the measurements which depends only on the hardware characteristics. As a result, the optimal value of ε is given by,

$$\varepsilon = w_{\max} \frac{\sigma_T}{\|T\|} \tag{22}$$

Lagier [5] details the exact derivation of Eq. (22) and shows that for typical thermal shock problems, $\|T\|$ needs to be evaluated at a non-dimensional time value equal to 1. The time scale is straightforwardly deduced from the other scales of the problem ($\tau = e^2\alpha$).

It can be noted that the reasoning leading to the optimal value of ε is analogous to the well known "L-curve" methodology. The threshold determination on ε relies exactly on the same idea: choose the hyperparameter value which makes the uncertainty on the solution resulting from the data uncertainty of the same magnitude as the rejected or truncated part of the solution. This is essentially similar to considering the respective magnitude of the residuals and the penalty term in the Tikhonov method for example. However, the advantage of the SVD algorithm shown here is that is does not require to plot explicitly the corresponding L-curve since the optimal value can be determined analytically.

As a conclusion, our method does not need any *a priori* information concerning the solution. Thus using the SVD regularization needs only the knowledge of the temperature measurements accuracy and no other information is required. Finally, only two hyperparameters namely the number of future time steps N_{pf} and the singularity threshold ε, are to be estimated. Besides, unlike the function specification method, no bias is introduced by the SVD technique and therefore the solution is not overly smoothed when large values of N_{pf} are used by the assumptions on the imposed temperature evolution. This is shown by Lagier [5] on a variety of analytical solutions. A too large number of future time steps in our method only results in longer computing times. Therefore N_{pf} will be chosen according to the explicit criterion exhibited by Lagier [5] and which has been validated by a sensitivity analysis.

The principle of the determination of the minimum value of N_{pf} is that the corresponding future time span, $N_{pf}\Delta t$, equals the required time for a heat shock to diffuse significantly on the length x separating the location of known values from those to be estimated, i.e., the thermal shock magnitude is several time larger than that of the measurement uncertainty scaled by σ_T. Lagier [5] showed that 5 times the temperature uncertainty was large enough to get results rather insensitive to larger values of N_{pf}. This non-dimensional time span is calculated considering a standard heat shock problem on a semi infinite wall with a sudden exposure to a given heat flux on the wall. The analytical solution to this problem is given, for example, by Luikov [6]. By expanding this solution for short times, the following non-dimensional evolution of the temperature is given

$$T^*(x,t) \approx \frac{4}{\sqrt{\pi}} \left(\frac{\sqrt{\alpha t}}{x} \right)^3 \exp\left(-\frac{x^2}{4\alpha t} \right) \tag{23}$$

This function is shown in Fig. 3. Another interesting consequence of the use of the SVD is to eliminate the need for a strictly determined set of equations. For example, it is possible to discretize very finely the boundary even though few internal temperatures are known. Using a threshold on the singular values discards also the singular vectors associated to a null singular value. As a consequence, it is possible to solve for underdetermined set of discretized equations with no loss of accuracy. This remark also means that it is no longer necessary to pay any particular attention to the number of discrete points on the boundary and to its relation to the number of sensors. The method provides the best possible estimate of the solution according to the threshold value. The only important consequence of

considering too many boundary points is a non-necessary increase in computing time.

3. Application to a two-dimensional case

3.1. Experimental set-up

To validate our method, an experimental setup named Cinthia, has been designed and built in our laboratory (Fig. 1). It was originally motivated by the need to cross-check the heat flux sensors of the Corine experiment with another heat flux determination method. The Corine experiment aims at describing the flow and heat transfer of a melt spreading on a cold wall in relation to severe accident studies for nuclear reactors. Depending on the operating conditions and considering the physical dimensions of the Cinthia setup, the heat diffusion problem in the vertical walls can be considered as one-dimensional or two-dimensional (Fig. 2).

The physical parameters describing the experiments are given in Table 1. The criterion for producing a one-dimensional diffusion situation is simply expressed in terms of the rising velocity of the liquid front, v, which must be much larger that the diffusion velocity scale, v_0, i.e.,

$$\frac{v}{v_0} \gg 1 \tag{24}$$

In the other situations, the diffusion is fully 2D. Five heat flux sensors are located on the inner surface of the stainless steel walls to measure the heat flux distribution due to the rising of the hot water front. These direct measurements are compared with numerical results obtained by solving the inverse problem. The data for the inverse problem are transient temperature measurements given by 15 thermocouples welded on the outer surface of the wall. All the boundaries except the one which is exposed to the heated fluid were insulated by using a 5 cm-thick layer of rock wool insulation around the test section (Kerlane, conductivity, 0.06 $W{\cdot}m^{-1}{\cdot}K^{-1}$). To be more precise the bottom part of the metal plates were mounted on a thermalite support, a particular material with a low conductivity (0.3 $W{\cdot}m^{-1}{\cdot}K^{-1}$). The influence of the heat losses on the result has not been studied and it has been simply assumed that the walls were perfectly insulated ($\frac{\partial T}{\partial n} = 0$).

3.2. Numerical results

In order to show the consistency of our algorithm, the inverse problem is first solved using analytical data. A numerical simulation of the heat flux distribution at the wall exposed to the hot liquid has been done. The rising speed is assumed to be constant and the rising time is equal to the typical diffusion time through the wall (see Table 1). In this situation, the diffusion problem is fully two-dimensional. The heat flux distribution resembles that of the

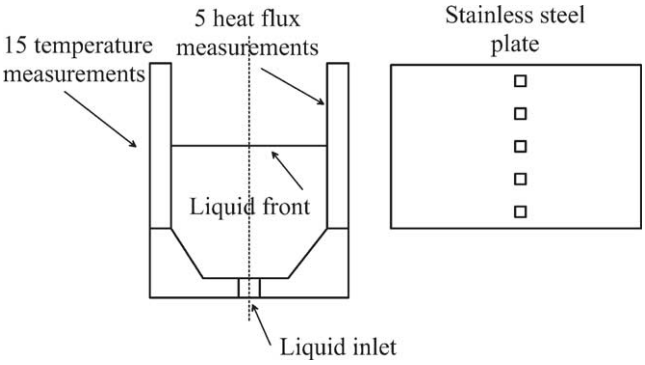

Fig. 1. Sketch of the Cinthia experiment. The flow of hot fluid comes from below. The instrumented walls are the two facing stainless steel plates. Their width is 35 mm, their height is 150 mm and their length is 300 mm. The lower parts and the sides are made of low conductivity material. The overall equipment is wrapped in a 5 cm thick rock wool layer. The plate walls facing the liquid are equipped with 5 heat flux sensors whereas on the other face 15 thermocouples are welded on the plate.

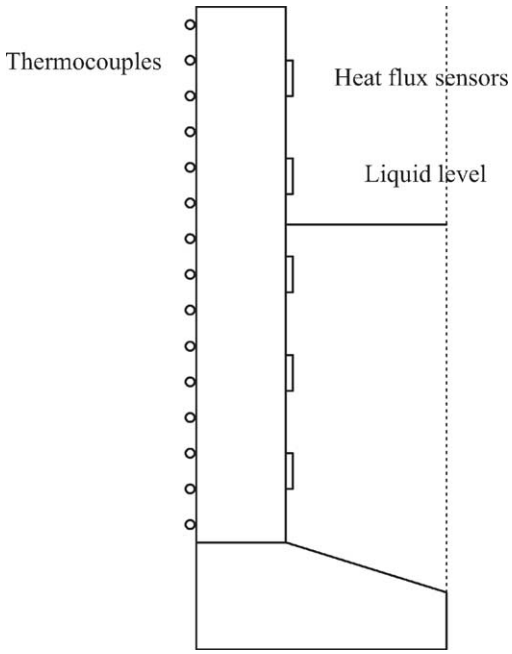

Fig. 2. Cinthia experiment. Detailed location of the sensors. The 15 type K thermocouples of 0.5 mm diameter. The hot liquid rises along the cold walls and produces a controlled heating and moving boundary.

Table 1
Physical parameters describing the diffusion problem in each wall of the Cinthia experiment

Characteristic length of diffusion (wall thickness e)	0.025 m
Thermal conductivity, k	16.3 $W{\cdot}m^{-1}{\cdot}K^{-1}$
Wall material density, ρ	7900 $kg{\cdot}m^{-3}$
Specific heat, c	500 $J{\cdot}kg^{-1}{\cdot}K^{-1}$
Thermal diffusivity, $\alpha = k/\rho c$	4.13×10^{-6} $m^2{\cdot}s^{-1}$
Characteristic diffusion time, $t_0 = e^2/\alpha$	152 s
Associated diffusion speed, $v_0 = e/t_0 = \alpha/e$	1.65×10^{-4} $m{\cdot}s^{-1}$

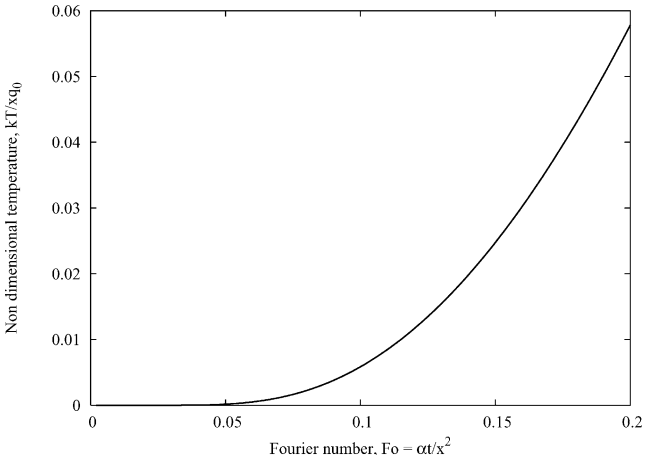

Fig. 3. Non-dimensional temperature rise at a distance x of the side of a semi infinite wall exposed suddenly at a constant heat flux. This function represents at small times the diffusion of a thermal shock on the boundary of a solid of finite size where the temperature sensors are located at a distance x from the wall end (see Eq. (23)).

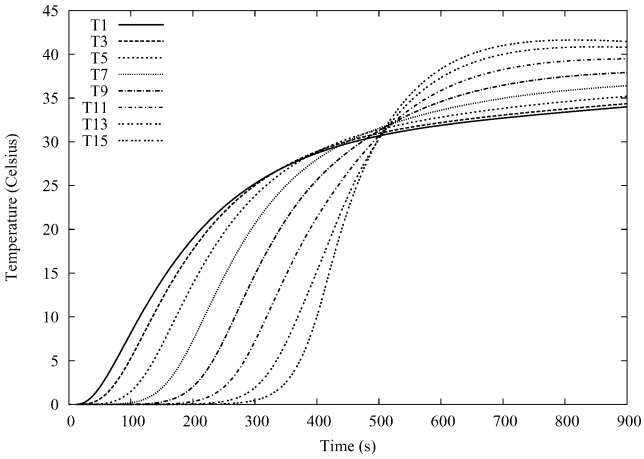

Fig. 4. Analytical temperatures for the two-dimensional inverse problem. The location of the thermocouples are shown in Fig. 2, they are numbered from the bottom to the top and only odd temperature data are shown for the sake of clarity.

experiments (see Figs. 8 and 12) and is only non-zero where the fluid wets the wall. The heat flux distribution is given by,

$$q(z,t) = q_0 \exp\bigl(-a(vt - z)\bigr) H(vt - z) \tag{25}$$

where $q_0 = 25$ kW·m^{-2}, $v = 3.75 \times 10^{-4}$ m·s^{-1}, $a = 20$ m^{-1} and where H denotes the Heaviside function. An analytical solution to the direct problem has been obtained by the method presented by Luikov [6]. As a consequence, *exact analytical temperatures* (Fig. 4) have been used when solving the inverse discretised problem. Furthermore, to mimic a more realistic situation, a Gaussian noise ($\sigma_{\text{noise}} = 0.1\,^\circ$C) has been added to the analytical values of the temperature. The value of the threshold for the SVD regularization given by (22) applied at $t = 150$ s, provides a value of $\varepsilon^* = 0.005$. All the calculations have been done with 300 time steps with $\Delta t = 3$ s ($\Delta t^* = \alpha \Delta t / e^2 \approx 0.02$) and 45 elements on the inner surface and 10 elements on the wall width.

Fig. 5 depicts the reconstructed heat flux values where the abscissa is the Fourier number which is the ratio of the physical time to the diffusion time scale t_0 given in Table 1 ($Fo = t/t_0$).

In Fig. 5, the heat flux peaks are clearly smoothed as already observed by Lagier [5] in simpler 1D cases. Peaks are associated with high frequency components of the solution, which are partly eliminated by the SVD truncation. Part of the high frequencies input due to the added Gaussian noise are suppressed, whereas some of them are still present in the calculated distribution as shown by the significant oscillations in reconstructed heat fluxes. In connection with these phenomena, it can be observed that the long-term evolution ($t^* > 4$) of the heat flux conflicts with common sense since it does not vanish identically. The space distribution of the heat flux, shown in Fig. 6, helps understanding this phenomenon. The analytical solution of the direct problem is given as an infinite series and the

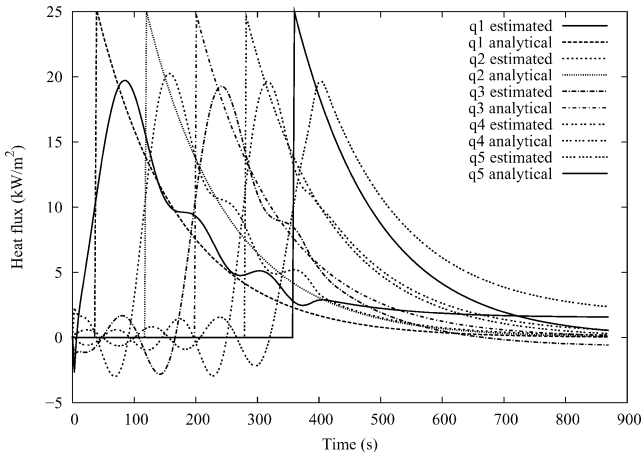

Fig. 5. Heat flux distribution reconstructed from noisy analytical data, (noise magnitude, 0.1 °C) ($\Delta t = 3$ s, $N_{pf} = 10$, $\varepsilon = 5 \times 10^{-3}$). The figure represents the comparison of the reconstructed heat flux and the analytical data (see Eq. (25)). The number of sensors and their location are shown in Fig. 2.

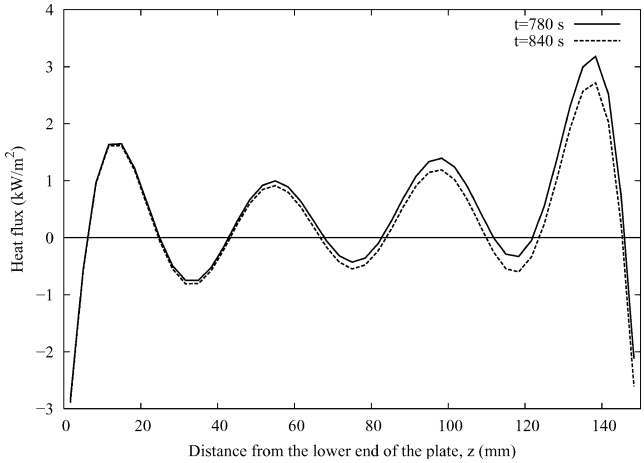

Fig. 6. Space distribution of the heat flux along the wall at long times, $t = 780$ and 840 s.

SVD regularization seems to truncate the solution to a finite number of these oscillating components. The spatial average of these oscillations seems rather small, which is consistent with the overall heat balance. However reducing further these oscillations does not seem possible since they are inherently linked to the truncation of the solution resulting from the unavoidable regularization. Fig. 5 must be borne in mind for the analysis of real data since it contains already most of the features to be shown on real data reconstruction.

3.3. Experimental results

Our algorithm is now applied to two experimental cases selected from the work of Lagier [5] namely run 16 and run 17. The heat flux is reconstructed from the evolution of the temperature at the location of the 15 thermocouples. The control parameters of the two experiments are given in Table 2. They are the initial wall temperature, the liquid temperature and the rise velocity of the front.

The temperatures measured during run 16 are shown in Fig. 7, whereas the heat flux measurements are shown in Fig. 8. According to Table 2, the rising velocity is high and the situation is therefore almost 1D. During the experiment, the rise velocity is almost constant, except near the end where the flow rate has been reduced to avoid the water to overflow the open box. This is clearly visible from the lagging temperature (T15 in Fig. 7) and flux (Flux-hfm-5, in Fig. 8). The temperature measurement uncertainty is approximately 0.1 °C.

Table 2
Control parameters of the two experiments described in Section 3.3

Parameter	Run 16	Run 17
Initial wall temperature [°C]	19	23
Water temperature [°C]	87	95
Temperature difference	68	72
Front velocity, v [m·s^{-1}]	10^{-2}	3.6×10^{-4}
Non-dimensional front velocity, v/v_0	61 (1D)	2.2 (2D)

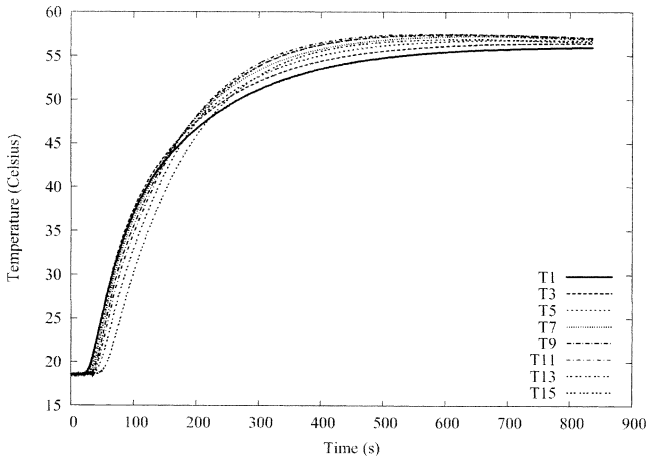

Fig. 7. Temperature measurements at odd temperature measurements locations (Cinthia run 16, see Table 1).

According to Eq. (22), the truncation threshold is $\varepsilon = 0.005$. Lagier [5] has shown it was also possible to find an *a priori* estimate of the hyperparameter for a variant of the Tikhonov method of order zero already used by Martin and Dulikravitch [8]. This variant may be substituted to our SVD-based procedure on the matrix of Eq. (11). The two hyperparameters of this former method are therefore N_{pf} and μ. For non-dimensional problems, it can be shown that the optimum hyperparameter value is,

$$\mu = \left(\frac{1}{2}\frac{\sigma_T}{\|T\|}\right)^2 \tag{26}$$

The derivation of this equation (see [5, Appendix 10]) follows the same path than that of Eq. (22). If consists in finding a bound for the uncertainty of he solution of the regularized method. This bound is made of two contributions analogous to those of Eq. (18). The optimum value of μ is based on the same argument: best compromise between noise amplification and loss of information. The corresponding value for the data of Fig. 7 is $\mu = 6.25 \times 10^{-6}$. The reconstructed heat flux is clearly one-dimensional, except for the 5th sensor for the reasons already mentioned. The Tikhonov regularization shown in Fig. 10 provides results similar to those of the SVD (Fig. 9), the former being slightly better at larger times. As already shown with the analytical data, the peaks are smoothed and the reconstruction seems of the same overall quality. Agreement with data seems correct at small times but seems to deteriorate at larger times since the heat flux does not vanish at long times (with respect to t_0). This initially unexpected trend is also shown by the analytical data and does not therefore result from the data quality.

The temperatures measured during Run 17 are shown in Fig. 11. During this experiment, the rise velocity is of the order of the diffusion velocity and the situation is fully two-dimensional. The data quality being similar to that of Run 16, the hyperparameters values are unchanged. The heat flux peaks are more severely smoothed in comparison to the previous quasi-1D case. The SVD reconstructed heat

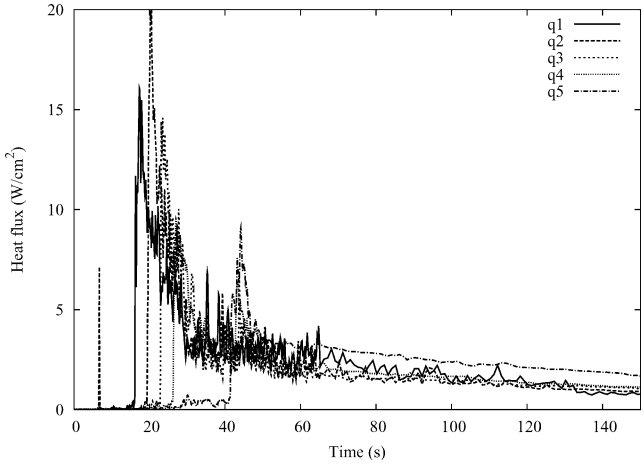

Fig. 8. Heat flux measurements at the 5 locations shown in Fig. 2 during run 16.

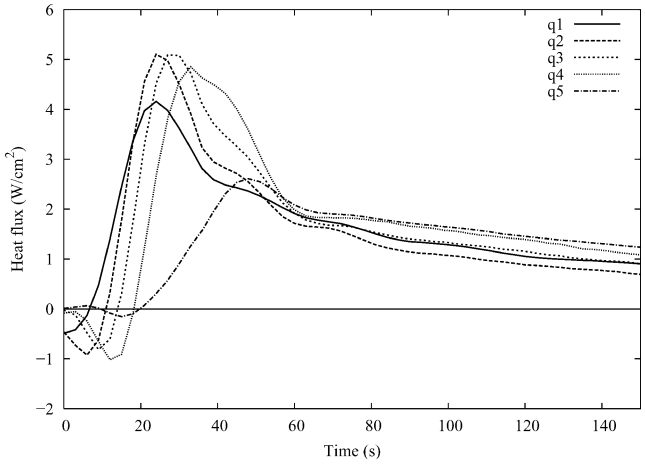

Fig. 9. Heat flux reconstructed at the flux meters location by the SVD algorithm (see Fig. 2). $N_{pf} = 10$, $\varepsilon = 0.005$.

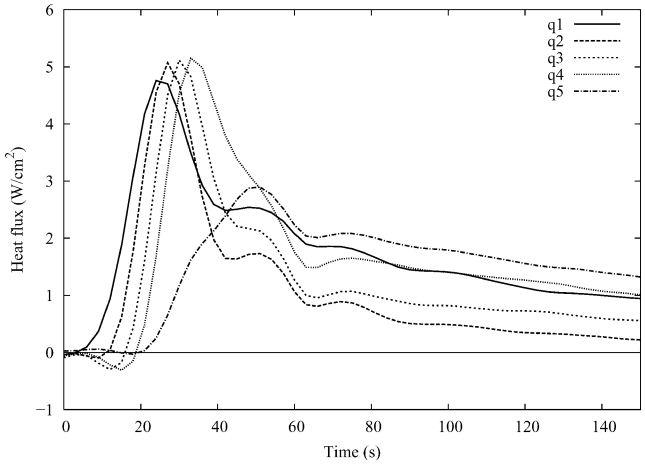

Fig. 10. Heat flux reconstructed at the flux meters location by the variant of Tikhonov regularization of order zero after Martin and Dulikravitch [8]. $N_{pf} = 10$, $\mu = 6.25 \times 10^{-6}$.

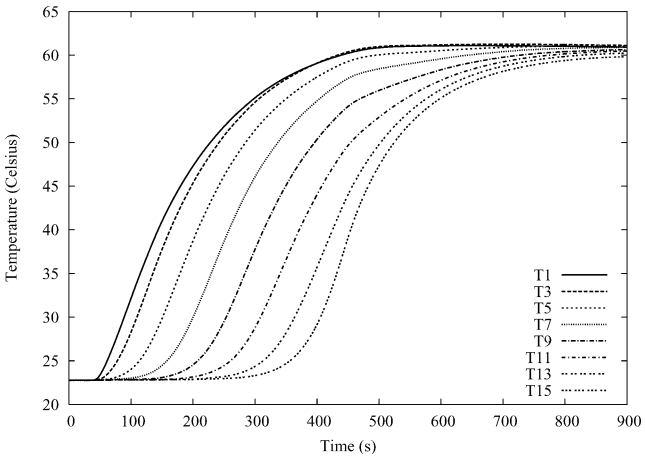

Fig. 11. Temperature measurements at odd temperature measurement locations (Cinthia run 17, see Table 2). Two-dimensional situation.

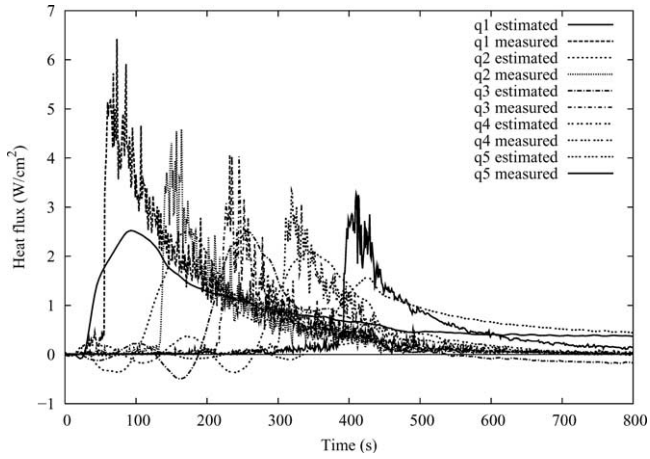

Fig. 12. Comparison between the reconstructed heat flux at the flux meters location by the SVD algorithm and the direct heat flux data (Cinthia run 17, see Table 2). $N_{pf} = 10$, $\varepsilon = 0.005$.

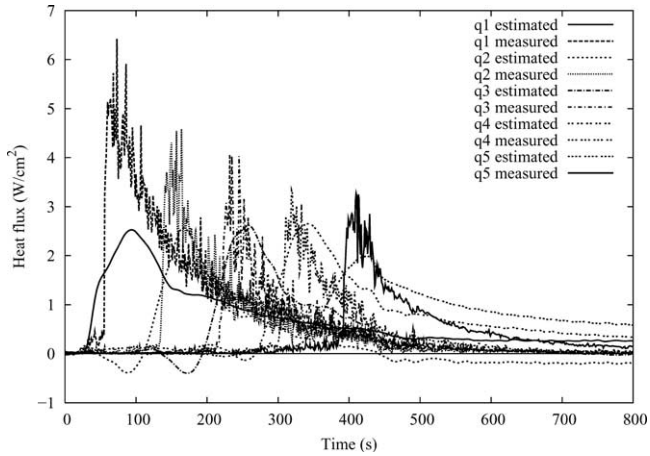

Fig. 13. Comparison between the measured hat flux and the estimated heat flux by the variant of the Tikhonov regularization of order zero after Martin and Dulikravitch [8] (Cinthia run 17, see Table 2). $N_{pf} = 10$, $\mu = 6.25 \times 10^{-6}$.

fluxes (Fig. 12) are not worse than those reconstructed by the Tikhonov method of order zero (Fig. 13). The long term trend of the heat flux already discussed with the previous data is always present and does not conflict with the previous analysis, however the unexpected low value of the first heat flux peak remains unexplained. The overall heat balance has been checked and is nevertheless verified.

Although, this has not been mentioned before, the criterion for the SVD method (Eq. (22)) has been intensively checked and eventually always calibrated with the residual principle. Fig. 13 shows the values of the temperature residual in the middle of the wall during Run 17. The residuals shown in Fig. 13 are defined as the difference between the actual temperature values (Fig. 10) and those reconstructed by solving the direct problem with a boundary condition based on the calculated heat flux (Fig. 11). It is expected from the theory that the resid-

ual must not exceed the noise amplitude (0.1 °C) and does not show any definite time evolution. Fig. 13 seems to clearly encompass all these features. Lagier [5] systematically checked these points for the 1D, 2D and 3D problems he solved.

4. Application of the methodology to a 3D test-case

The purpose of this section is to show that the presented methodology can be applied to 3D cases as well with no modification. The test case to be solved is the following. Let us consider the same stainless steal plate already considered in the Cinthia experiment. Its thickness is $e = 25$ mm in the z direction, its width is $L = 300$ mm in the y direction and its height is $l = 150$ mm in the x direction. Instead of applying a heat flux with a moving boundary ($x(t)$) on the whole surface of the plate, let us heat the plate only on a central strip of width ($-L < -L_0 \leqslant y \leqslant L_0 < L$). The problem being even in the y direction it is only necessary to consider the $y > 0$ part of the plate. This is accounted for by a method similar to that of the image method for Laplace equation. Let us further assume that all the other walls are perfectly insulated. The heat flux applied on the exposed face of the wall is similar to the 2D case (see Eq. (25)) and is now given by,

$$q(x, y, t) = \begin{cases} q_0 \exp\bigl(-a(vt - x)\bigr) H(vt - x) \\ \quad 0 \leqslant y \leqslant L_0 \\ 0 \\ \quad L_0 < y < L \end{cases} \tag{27}$$

where the previously mentioned values of the parameters are, the maximum heat flux $q_0 = 50$ kW·m^{-2}, the front rise velocity is $v = 0.5$ mm·s^{-1} and the spatial decay of the heat flux is $a = 40$ m^{-1}. In this particular problem, $L_0 = 100$ mm has been chosen, so that two-thirds of the plate are exposed to the heat flux. Lagier (see [5, Appendix 9]) exhibited an analytical solution to this problem which will be used further as the input data for the inverse problem.

For the inverse problem, it has been assumed that 144 temperatures can be measured on the rear side of the plate. The plate surface meshing is made of 12×12 identical rectangular elements whereas 4 elements were included in the thickness of the plate. The total number of elements is 432. Considering the smallest size of the elements, the time step is chosen according to Eq. (13) which provides $\Delta t = 5$ s. The number of future time steps is set to $N_{pf} = 5$, following the same procedure than for the 2D case.

Fig. 15 shows the analytical values of the temperature calculated at various locations on the rear side of the plate. The earlier the temperature rises, the lower (in x direction) are located the temperature probes. In the vicinity of the vertical symmetry plane of the plate ($y = 0$), the temperature rises quite independently of the distance to this plane;

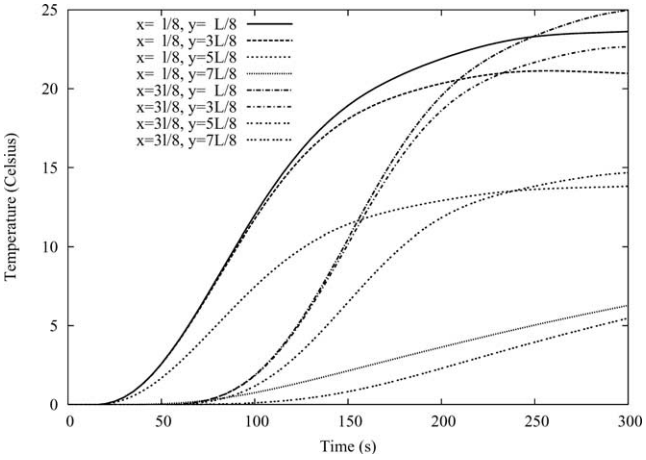

Fig. 15. Calculated 3D temperature evolutions at selected points of the rear face of the plate. Analytical calculation to be used as an input for the inverse problem.

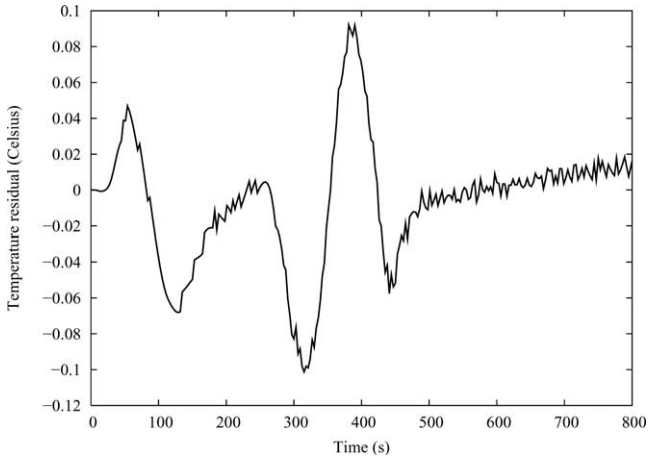

Fig. 14. Temperature residue at location T8 (middle of the wall) for the reconstructed flux by the SVD in Run 17.

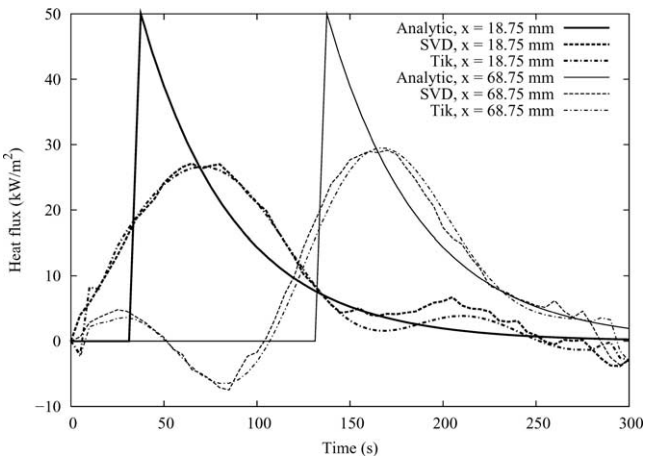

Fig. 16. Comparison between the analytical and the reconstructed heat flux values by the SVD method ($\varepsilon^* = 0.01$, $N_{pf} = 5$) and the variant of the Tikhonov method of order 0 utilized by Martin and Dulikravitch [8] close to the symmetry plane of the plate ($y = 18.75$ mm) at two different levels ($x = 18.75$ mm and $x = 68.75$ mm).

whereas when the sensor is located closer to the plate end ($y = L$), lateral diffusion is significant. The temperature evolutions are similar for thermocouples located at higher elevations with a significant delay simply related to the rise time of the liquid front.

5. Conclusions

In this paper, we have proposed and discussed a new method which is based on a boundary element formulation for solving multidimensional unsteady inverse heat conduction problem. We emphasize the fact that only two hyperparameters have to be estimated, and no *a priori* information is required on the time evolution of the solution. Estimates of these hyperparameters are possible from the known values of the scales of the problem and the data uncertainty according to the criteria originally derived by Lagier [5].

In this paper, we have applied our method to a two-dimensional case, using simulated (analytical) and experimental data. It has been shown than the same methodology can be applied directly to 3D problems. The few sample calculations presented here show that SVD can be used as a very versatile regularization technique and yields results of quality comparable to some other widely used regularization methods. This regularization method does not depend on the space dimension, and can be uniformly applied from 1D to 3D problems. It has been shown that 3D problems can be solved using the same approach, however, its experimental validation would require a tremendous amount of data that cannot be produced by using few tens of thermocouples. Infrared thermography may provide the appropriate amount of input data relative 3D problems. There is therefore a strong interest in designing a benchmark experiment using IR technology for the validation of our method in real 3D situations.

Acknowledgement

The authors acknowledge the input of M. Samaille, J.M. Veteau and Y. Bernard from CEA/DTP for the experimental part of this work.

References

[1] O.M. Alifanov, E.A. Artyukhin, S.V. Rumyantsev, Extreme Methods for Solving Ill-Posed Problems with Applications to Inverse Heat Transfer Problems, Begell House, New York, 1995.
[2] J.V. Beck, B. Blackwell, C.R. Saint-Clair, Inverse Heat Conduction—Ill-Posed Problems, Wiley, New York, 1985.
[3] P.C. Hansen, Rank-Deficient and Discrete Ill-Posed Problems, SIAM, Philadelphia, PA, 1998.
[4] Y. Jarny, D. Maillet, Les problemès inverses en thermique, cours C de l'école de printemps METTI, GUT Aussois, March 19–25, 1995.
[5] G.L. Lagier, Application de la méthode des éléments de frontières à la résolution du problème inverse de conduction de la chaleur multidimensionnel, stationnaire et instationnaire. Régularisation par troncature de spectre, Ph.D. Thesis, Institut National Polytechnique de Grenoble, spécialité énergétique, 1999.
[6] A.V. Luikov, Analytical Heat Diffusion, Academic Press, New York, 1968.
[7] D. Maillet, A. Degiovanni, R. Pasquetti, Inverse heat conduction applied to the measurement of heat transfer coefficient on a cylinder: Comparison between an analytical and a boundary element technique, J. Heat Transfer 113 (1991) 549–557.
[8] T.J. Martin, G.S. Dulikravitch, Inverse determination of boundary conditions and sources in steady heat conduction with heat generation, J. Heat Transfer 118 (1996) 546–554.
[9] A.J. Novak, A.C. Newes, The Multiple Reciprocity Boundary Element Method, Computational Mechanics Publications and Elsevier, 1994.
[10] R. Pasquetti, C. Le Niliot, Boundary element approach for inverse heat conduction problems: Application to a bidimensional transient numerical experiment, Numer. Heat Transfer B 20 (1991) 169–189.
[11] W.H. Press, S.A. Teukolski, W.T. Vetterling, B.P. Flannery, Numerical Recipes in C, second ed., Cambridge University Press, Cambridge, 1992.
[12] A.N. Tikhonov, V.Y. Arsenin, Solution of Ill-Posed Problem Solution, Winston and Sons, Washington, DC, 1977.